

Dislocation Mobility in a Quantum Crystal: the Case of Solid ^4He

Renato Pessoa,^{*} S. A. Vitiello,[†] and Maurice de Koning[‡]

Instituto de Física Gleb Wataghin, Caixa Postal 6165,

Universidade Estadual de Campinas - UNICAMP 13083-970, Campinas, SP, Brazil

(Dated: April 2, 2022)

Abstract

We investigate the structure and mobility of dislocations in *hcp* ^4He crystals. In addition to fully characterizing the five elastic constants of this system, we obtain direct insight into dislocation core structures on the basal plane, which demonstrates a tendency toward dissociation into partial dislocations. Moreover, our results suggest that intrinsic lattice resistance is an essential factor in the mobility of these dislocations. This insight sheds new light on the possible correlation between dislocation mobility and the observed macroscopic behavior of crystalline ^4He .

Dislocations are line defects that play a central role in the mechanical deformation behavior of crystalline solids [1]. Their activity is widely known to be pivotal in classical solids, controlling phenomena such as fracture and brittle-ductile transitions in metals and semiconductors. Much less is known [2], however, about the influence of dislocations on the properties of quantum crystals, which are solids where the quantum-mechanical zero-point kinetic energy is significant compared to the typical energy scale of the interatomic interactions [3].

Recent experimental studies on crystalline solid ^4He , the prototypical quantum solid, indirectly indicate that dislocations are indeed involved in macroscopic phenomena. The occurrence of apparent superfluidity [4, 5] and the observation of elastic stiffening [6–8], for instance, have been linked to the mobility of dislocations. However, in contrast to classical solids, for which an abundant body of experimental results exists, the lack of specific experimental data concerning the behavior of dislocations prevents a direct investigation of this relationship. In view of these difficulties, one needs to resort to theoretical approaches. In principle, a realistic picture of dislocations and their properties is possible using path-integral or variational Monte Carlo simulations. However, given that dislocation modeling requires a simultaneous treatment of different length scales [9], one associated with the core properties and the other associated with distances large compared to the atomic scale, the viability of these direct approaches remains a subject of debate [10–12].

In this Letter, adopting a methodology that incorporates both of the relevant scales, we obtain fundamental insight into the properties of dislocations in the archetypal quantum crystal: solid *hcp* ^4He . We compute the intrinsic dislocation structure and mobility of four different dislocation types using the multiscale paradigm of the semi-discrete Peierls-Nabarro (PN) model [13–15]. It constitutes a hybrid continuum-atomistic approach that captures the long-range elastic fields as well as the lattice-discreteness effects associated with the dislocation core. All parameters in the model are determined using quantum-mechanical expectation values for ^4He applying the shadow wave function (SWF) formalism [16, 17]. In addition to providing key information concerning the elastic properties, our results shed new light onto the possible role of dislocations in the experimental observation of the elastic stiffening of solid and its potential connection to the apparent superfluidity in this quantum crystal.

Within the semi-discrete PN framework, a straight dislocation lying along the y -direction

is represented in terms of a set of misfit vectors $\vec{\delta}_i$ that describe the disregistry of atomic row i relative to their counterparts on the other side of the glide plane, as depicted in Fig.1. Panel a) shows a schematic representation of two sets of atomic rows extending along the y -direction, one set on each side of the glide plane. The rows above the plane are labeled by the index i . Panel b) shows a top view, depicting a disregistry vector $\vec{\delta}_i$ for row i . In this manner, the total misfit associated with a given dislocation, described by the Burgers vector \vec{b} , is thought of as distributed among the atomic rows along the x -axis, subject to the boundary conditions $\vec{\delta}_{-\infty} = 0$ and $\vec{\delta}_{\infty} = \vec{b}$. Here, we consider two-dimensional misfit vectors $\vec{\delta}_i = \delta_i^e \hat{x} + \delta_i^s \hat{y}$, with edge and screw components along the x and y directions, respectively. The equilibrium structure of the dislocation is then represented by that particular misfit distribution $\vec{\delta}_i$ that minimizes the dislocation energy per unit length,

$$U_{\text{disl}} = U_{\text{elastic}} + U_{\text{misfit}} + U_{\text{stress}} + C, \quad (1)$$

where

$$U_{\text{elastic}} = \sum_{i,j} \chi_{ij} (K_e \rho_i^e \rho_j^e + K_s \rho_i^s \rho_j^s), \quad (2)$$

$$U_{\text{misfit}} = \sum_i \gamma(\vec{\delta}_i) \Delta x, \quad (3)$$

$$U_{\text{stress}} = \frac{1}{2} \sum_i [\tau^e (\delta_i^e + \delta_{i-1}^e) + \tau^s (\delta_i^s + \delta_{i-1}^s)] \Delta x, \quad (4)$$

and C is a constant that can be ignored [13]. In the elastic part of the dislocation energy, Eq. (2), χ_{ij} is a discretized universal kernel [14], and $K_e = \mu/4\pi(1 - \nu)$ and $K_s = \mu/4\pi$ are elastic pre-factors with μ the shear modulus and ν the Poisson's ratio. In addition, $\rho_i^e \equiv (\delta_i^e - \delta_{i-1}^e) / \Delta x$ and $\rho_i^s \equiv (\delta_i^s - \delta_{i-1}^s) / \Delta x$, where Δx is the distance between adjacent rows in the defect-free crystal. Eq.(3) represents the misfit contribution, in which $\gamma(\vec{\delta})$ is known as the generalized stacking-fault (GSF) energy surface [18]. It describes the excess energy per unit area of a crystal that is subjected to the following procedure. It is first cut into two defect-free parts across a given plane. The two parts are then displaced relative to each other by a vector $\vec{\delta}$, after which they are patched together again. An example configuration of the GSF on the basal plane of the *hcp* structure is the intrinsic stacking fault (ISF), in which the displacement vector $\vec{\delta}$ describes the associated shift in the planar stacking.

In the context of the PN model, the GSF surface reflects the inter-atomic interactions in the system and serves to model the details of the dislocation core on the atomic scale. Finally, the stress term of Eq. (4) accounts for the work done by any external stresses, where τ^e and τ^s denote the magnitude of the components of the stress tensor that couple to the edge and screw displacements, respectively [1]. The quantities that specify the model for dislocations in a particular material are the elastic parameters μ and ν , the GSF surface $\gamma(\vec{\delta})$ associated with the glide plane of interest, and Δx .

Here, we employ the SWF model based on the parameter set of Ref.[17] to determine these quantities for solid *hcp* ^4He (space group 194). In order to determine its elastic properties, we employ a computational cell containing 720 particles at a density of 0.0294 \AA^{-3} , which corresponds to lattice parameters $a=3.63668 \text{ \AA}$ and $c=5.93866 \text{ \AA}$, subject to standard periodic boundary conditions. Sampling configurations according to the quantum-mechanical probability density of the SWF model using the Metropolis algorithm, we then compute expectation values of the stress tensor [19] associated with the six independent deformations of the periodic cell, imposing strain levels of 0.25%. Using the standard relationship between the stress and strain tensors [20], we extract the five independent elastic constants of the *hcp* structure. The results, which, to the best of our knowledge represent the first complete estimate of the elastic constants in *hcp* ^4He , are reported in Table I. The shear modulus $\mu = C_{44} = 17.1 \pm 0.8 \text{ MPa}$, is in good agreement with the value of 14 MPa that follows from the ratio of the experimental shear stress and strain values reported in [21]. Poisson's ratio, obtained from the results in Table I, is found to be $\nu = 0.151$. Both theoretical values are those corresponding to shear directions in the basal plane, in which hexagonal crystals are isotropic [22].

Since basal slip is known to be the dominant dislocation glide mechanism in *hcp* solid ^4He [23] we focus on the properties of these particular dislocations and compute the GSF surface associated with the basal plane. For this purpose, we utilize the 720-atom cell and impose a series of 400 slip vectors $\vec{\delta}$ in the basal plane by adjusting the periodic boundary condition along the *c*-axis. The shadow degrees of freedom of the atoms immediately adjacent to the slip plane are allowed to vary only along the *c*-direction to maintain the relative displacement. Using the Metropolis algorithm we then sample configurations according to the SWF and compute the expectation value of the Hamiltonian as a function of $\vec{\delta}$. Subtracting the expectation value at $\vec{\delta} = 0$ and dividing by the area, we then obtain the GSF surface.

In order to implement the results into the PN mode, we fit the results using a Fourier series that reflects the lattice symmetry of the basal plane of the *hcp* structure: $\gamma(\vec{\delta}) = \sum_{\vec{G}} c_{\vec{G}} \exp(i\vec{G} \cdot \vec{\delta})$, in which we use a set of 81 two-dimensional reciprocal lattice vectors \vec{G} . The results are shown in Fig. 2. The perfect crystal configuration, which has GSF value of zero, is associated with the displacement $\vec{\delta} = 0$ and its periodic equivalents. The ISF configuration, which corresponds to the displacement vector (and equivalents) $\vec{\delta} = (0, b_p)$, with $b_p = \frac{1}{3}\sqrt{3}a = 2.0996 \text{ \AA}$ the length of a partial Burgers vector, has an excess energy of 0.0063 mJ/m^2 .

Using our estimates for the elastic properties and the GSF surface in the PN model, we investigate the structure and intrinsic mobility of 4 dislocation types on the basal plane: (i) screw, (ii) 30° , (iii) 60° , and (iv) edge. Fig. 3 shows the optimized disregistry profile for the screw dislocation, obtained by minimizing Eq. (1) at zero external stress. As expected, given the low stacking-fault energy (SFE) value, it dissociates into two 30° partial dislocations with opposite edge components, separated by an ISF area with a width of 29 atomic rows, which corresponds to 91.33 \AA . The core width ς of the partials, defined as the distance over which the displacement changes from $\frac{1}{4}$ to $\frac{3}{4}$ of its total value[14], is approximately 1 atomic row or $\sim 3.1 \text{ \AA}$. The second line of Table II contains the dissociation widths of the other three dislocations, showing an increasing ISF width with increasing edge component, consistent with dislocation theory [1].

In addition to the structural properties described here, the PN model permits an estimate of the intrinsic dislocation mobility, which is measured in terms of the Peierls stress. To this end, we impose an external shear stress in the glide plane parallel to the total Burgers vector. It produces maximal force per unit length [1] on the dislocation line for the given stress magnitude. This magnitude is then increased in small steps, followed by minimization of Eq. (1) with respect to the disregistry vectors $\vec{\delta}_i$. At a critical stress value, the so-called Peierls stress, an instability is reached and an equilibrium solution ceases to exist.[14, 15] In this situation the dislocation becomes free to move through the crystal. The third line of Table II contains the Peierls stress values for the four considered dislocation types. The lowest Peierls stress value, obtained for the 30° dislocation, is of the order of $1.5 \times 10^{-2} \text{ MPa}$. This value is ~ 3 orders of magnitude smaller than the shear modulus, which is consistent with the typical discrepancy between the ideal shear strength and actual yield stresses in crystals [1].

The above results were obtained using the SWF model, which, while providing a good description of the shear modulus for *hcp* solid ^4He , significantly underestimates a recent experimental estimate for the SFE, $(0.07 \pm 0.02) \text{ mJ/m}^2$ [24]. In order to explore the possible influence of the SFE value on the dislocation mobility, we repeat the Peierls stress calculations for the case in which the equilibrium dissociation widths of the four dislocation types is reduced by a factor 10, which is the ratio between the experimental and theoretical SFE values. To this end, we apply an additional shear stress component, whose direction in the glide plane is perpendicular to the total Burgers vector of the dislocation. This stress component, known as Escaig stress [9], does not produce a force on the dislocation as a whole, but mimics a situation with a different SFE value. Using an Escaig stress of 0.4 MPa, we recompute the Peierls stress values for the four dislocations types in the basal plane. The results are shown in the fourth row of Table II. The effect of an increased effective SFE value does not significantly affect the Peierls stress values of the model. This is consistent with earlier PN calculations in metals, in which the Peierls stress was not found to be sensitive to dissociation width [14].

Finally, we examine our results in the context of recent experiments considering the macroscopic behavior of solid ^4He at low temperatures. In the observation [4, 5] of non-classical rotational inertia (NCRI), interpreted as a signature of superfluidity, the crucial role of crystal defects and disorder seems firmly established. Specifically, the behavior of dislocations has attracted a particular interest after the discovery of an unexpected increase of the shear modulus that shows the same temperature and ^3He impurity concentration dependence as the original NCRI observations [6–8]. Inspired by the continuum-elasticity based Granato-Lücke theory [25], it has been hypothesized that this stiffening is a consequence of a change of mobility of a network of dislocations. This network is thought to be pinned by ^3He impurities at lowest temperatures, while it becomes mobile under warmer conditions. Analyzing the dislocation mobility results of our model, it is interesting to observe that our lowest Peierls barrier is about 20 times *larger* than the shear stresses of $\sim 700 \text{ Pa}$ reached in recent experiments [7]. This suggests that intrinsic lattice resistance is an essential factor when it comes to the mobility of dislocations on the basal plane in *hcp* solid ^4He . Indeed, at the stress levels reported in these recent experiments, such dislocations would not be expected to be mobile, not even in the absence of any pinning centers. Moreover, it is not expected that the Peierls stress varies significantly as a function of temperature below 0.1 K,

at which the stiffening is observed, given that finite temperature path-integral Monte Carlo calculations of several properties do not show a significant temperature dependence below 1 K [26]. In this context, a satisfactory explanation for the observed elastic stiffening in *hcp* solid ^4He must involve intrinsic mobility issues.

In summary, we employ a hybrid continuum-atomistic approach, based on the Peierls-Nabarro model and the shadow wave function formalism, to obtain direct insight into the intrinsic structural and mobility properties of dislocations in *hcp* solid ^4He at zero temperature. In addition to providing key information concerning the elastic properties of this prototypical quantum crystal, the results reveal a significant lattice resistance to dislocation motion. Analyzing our results in the context of the proposed dislocation-pinning interpretation of the similarity between the NCRI and elastic stiffening phenomena suggests that intrinsic lattice resistance is an essential factor when it comes to the mobility of dislocations. The proposed interpretation, which entirely ignores this element, may therefore not provide a satisfactory explanation for the observed elastic stiffening in *hcp* solid ^4He .

The authors acknowledge financial support from the Brazilian agencies FAPESP, CNPq and CAPES. Part of the computations were performed at the CENAPAD high-performance computing facility at Universidade Estadual de Campinas.

* Electronic address: rpessoa@ifi.unicamp.br

† Electronic address: vitiello@unicamp.br

‡ Electronic address: dekonig@ifi.unicamp.br

- [1] J. P. Hirth and J. Lothe, *Theory of Dislocations* (Wiley, New York, 1982), 2nd ed.
- [2] S. Balibar, *Nat Phys* **5**, 534 (2009).
- [3] P. W. Anderson, *Basic Notions of Condensed Matter Physics* (Benjamin-Cummings, 1984).
- [4] E. Kim and M. H. W. Chan, *Science* **305**, 1941 (2004).
- [5] E. Kim and M. H. W. Chan, *Nature* **427**, 225 (2004).
- [6] J. Day and J. Beamish, *Nature* **450**, 853 (2007).
- [7] J. Day, O. Syshchenko, and J. Beamish, *Phys. Rev. B* **79**, 214524 (2009).
- [8] J. T. West, O. Syshchenko, J. Beamish, and M. H. W. Chan, *Nat Phys* **5**, 598 (2009).
- [9] V. V. Bulatov and W. Cai, *Computer simulations of dislocations* (Oxford University Press,

- 2006).
- [10] P. W. Anderson, *Science* **324**, 631 (2009).
 - [11] M. Boninsegni, A. B. Kuklov, L. Pollet, N. V. Prokof'ev, B. V. Svistunov, and M. Troyer, *Phys. Rev. Lett.* **99**, 035301 (2007).
 - [12] L. Pollet, M. Boninsegni, A. B. Kuklov, N. V. Prokof'ev, B. V. Svistunov, and M. Troyer, *Phys. Rev. Lett.* **98**, 135301 (2007).
 - [13] V. V. Bulatov and E. Kaxiras, *Phys. Rev. Lett.* **78**, 4221 (1997).
 - [14] G. Lu, N. Kioussis, V. V. Bulatov, and E. Kaxiras, *Phys. Rev. B* **62**, 3099 (2000).
 - [15] G. Lu, V. V. Bulatov, and N. Kioussis, *Phil. Mag.* **83**, 3539 (2003).
 - [16] S. Vitiello, K. Runge, and M. H. Kalos, *Phys. Rev. Lett.* **60**, 1970 (1988).
 - [17] T. MacFarland, S. A. Vitiello, L. Reatto, G. V. Chester, and M. H. Kalos, *Phys. Rev. B* **50**, 13577 (1994).
 - [18] V. Vitek, *Philos. Mag.* **18**, 773 (1968).
 - [19] D. Ceperley, G. V. Chester, and M. H. Kalos, *Phys. Rev. B* **16**, 3081 (1977).
 - [20] J. F. Nye, *Physical Properties of Crystals: Their Representation by Tensors and Matrices* (Oxford University Press, 1985).
 - [21] O. Syshchenko, J. Day, and J. Beamish, *J. Phys.: Condens. Matter* **21**, 164204 (2009).
 - [22] Y. Li, *Phys. Stat. Sol. (a)* **38**, 171 (1976).
 - [23] M. A. Paalanen, D. J. Bishop, and H. W. Dail, *Phys. Rev. Lett.* **46**, 664 (1981).
 - [24] H. J. Junes, H. Alles, M. S. Manninen, A. Y. Parshin, and I. A. Todoshchenko, *J. Low. Temp. Phys.* **153**, 244 (2008).
 - [25] A. Granato and K. Lücke, *J. Appl. Phys.* **27**, 583 (1956).
 - [26] D. M. Ceperley, *Rev. Mod. Phys.* **67**, 279 (1995).

Table I: Elastic constants of the SWF model for *hcp* ^4He within the SWF model, in units of MPa.

C_{11}	C_{33}	C_{44}	C_{12}	C_{13}
60.8 ± 0.8	77.9 ± 0.8	17.1 ± 0.8	34.4 ± 0.8	14.4 ± 0.8

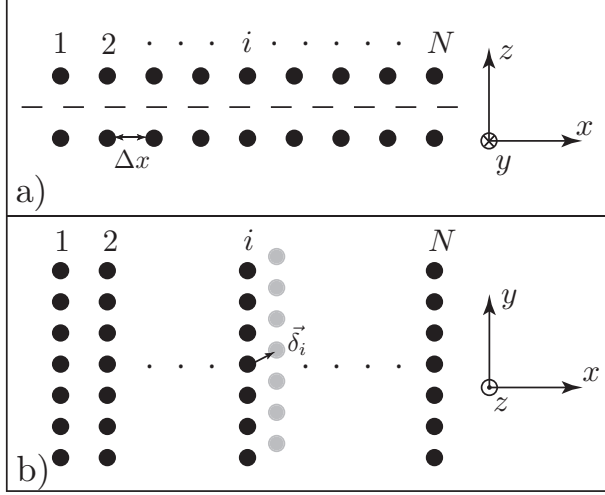


Figure 1: Degrees of freedom in the PN model. a) Atomic rows on one side of slip plane (dashed line) are labeled by index i . Distance between adjacent rows in defect-free crystal is Δx . b) Displacements of rows with respect to those on other side of slip plane are described by vector $\vec{\delta}_i$.

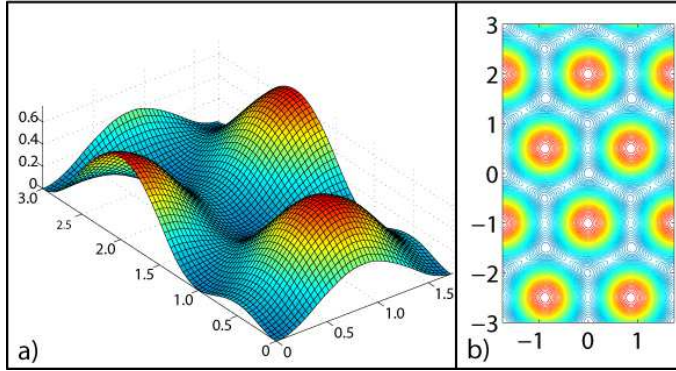


Figure 2: Fourier series representation of GSF surface on the basal plane of hcp ^4He as modeled by the SWF model. a) GSF energy (in mJ/m^2) as a function of two-dimensional displacement $\vec{\delta}$ (in units of $b_p = \frac{1}{3}\sqrt{3}a = 2.0996 \text{ \AA}$). b) Contour plot of GSF surface reflects symmetry of basal plane of hcp surface.

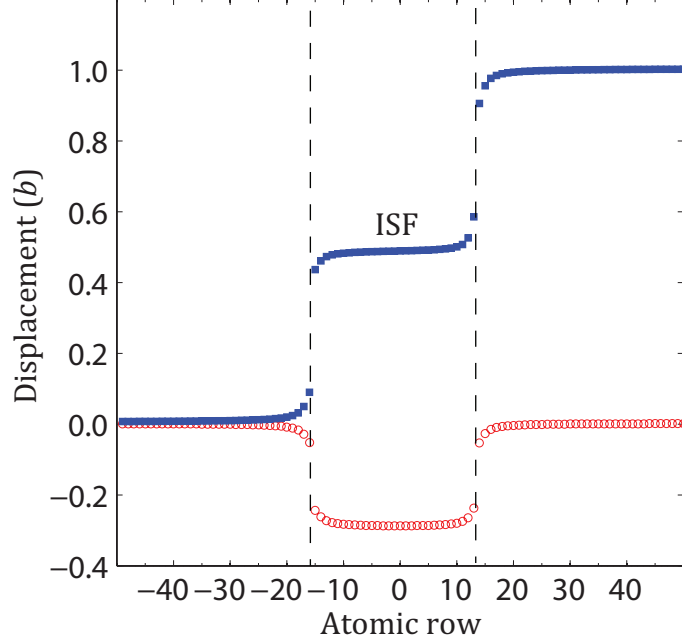


Figure 3: Optimized displacement profile $\vec{\delta}_i$ for screw dislocation on basal plane: edge component (open circles) and screw component (filled squares) are measured in units of the Burgers vector $b = a = 3.63668\text{\AA}$. Dashed lines indicate positions of partial dislocations.

Table II: Core structure and Peierls Stress for four dislocations on the basal plane for the SWF model for solid *hcp* ^4He .

	Screw	30°	60°	Edge
Partial separation (\AA)	91.3	109.1	119.7	127.3
Peierls Stress (MPa)	0.41 ± 0.01	0.015 ± 0.01	0.23 ± 0.01	0.08 ± 0.01
Peierls Stress corrected SFE (MPa)	0.48 ± 0.01	0.045 ± 0.01	0.39 ± 0.01	0.08 ± 0.01